Supplementary Information

Efficient polymer acceptor *via* random polymerization strategy enables all polymer solar cells with efficiency exceeding 17%

Yun Li,‡[a] Qian Li,‡[b] Yunhao Cai,*[a] Hui Jin,[c] Jianqi Zhang,[d] Zheng Tang,[c] Chunfeng Zhang,[b] Zhixiang Wei,[d] and Yanming Sun*[a]

[a]School of Chemistry, Beihang University, Beijing 100191, P. R. China, E-mail: caiyunhao@buaa.edu.cn; sunym@buaa.edu.cn

[b]National Laboratory of Solid State Microstructures, School of Physics, and Collaborative Innovation Center for Advanced Microstructures, Nanjing University, Nanjing 210093, P. R. China

[c]State Key Laboratory for Modification of Chemical Fibers and Polymer Materials, Center for Advanced Low-dimension Materials,College of Materials Science and Engineering,Donghua UniversityShanghai, 201620, P. R. China

[d]CAS Key Laboratory of Nanosystem and Hierarchical FabricationCAS Center for Excellence in NanoscienceNational Center for Nanoscience and TechnologyBeijing 100190, P. R. China

† Electronic supplementary information (ESI) available

‡ Y. Li and Q. Li contributed equally to this work.

Materials: PM6 was purchased from Solarmer Inc., and all reagents and chemicals were purchased from Energy Chemical used without further purification. Compound of 5,6-dinitro-4,7-bis(6-undecylthieno[3,2-b]thiophen-2-yl)benzo[c][1,2,5]thiadiazole was synthesized according to previously reported literature.[1]

Synthesis of compound SMA-C11

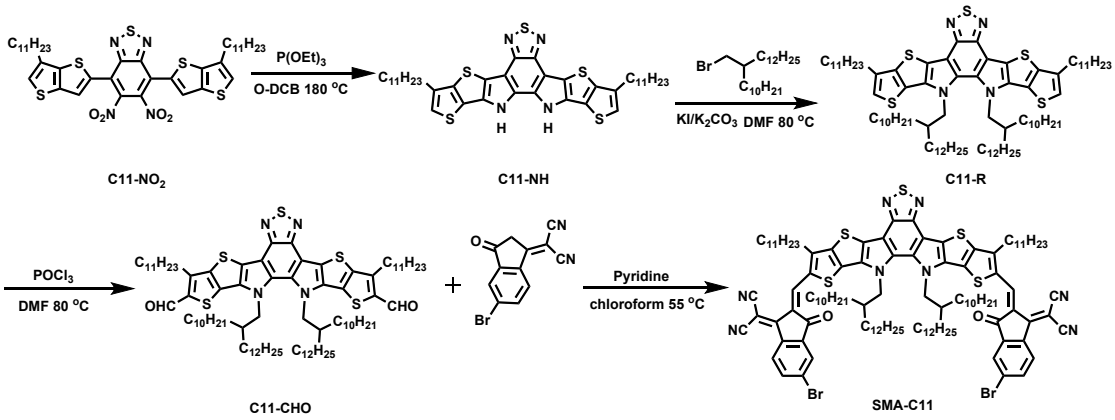

Scheme S1. The synthetic route of SMA-C11.

Compound C11-R: Under nitrogen protection, $P(OEt)_3$ (3.5 mL) was added to the solution of compound C11-NO_2 (1.02 g, 1.26 mmol,) in o-DCB (32 mL). The reaction mixture was heated to reflux at 180 °C and stirred 10 h. After cooling to room temperature, the solvent was removed under reduced pressure and the residue was added to 100 mL two-necked round bottom flask which containing 11-(bromomethyl)tricosane (7.87 g, 18.9 mmol)/ K_2CO_3 (2.02 g, 14.65 mmol), KI (2.50 g, 15.07 mmol) and DMF (48 mL). The reaction mixture was heated at 80 °C and stirred overnight. After cooling to room temperature, the mixture was added water and extracted with dichloromethane for three times. The combined organic phase was further washed with water, and dried with anhydrous $MgSO_4$, filtrated and concentrated under reduced pressure. The residue was purified with column chromatography on silica gel. The eluent is PE: DCM = 9:1 (v:v). The final product compound C11-R was obtained as an orange solid (1.00 g, 56%).

C11-CHO: Under nitrogen protection, $POCl_3$ (0.5 mL) was added dropwise to a solution of anhydrous N,N-Dimethylformamide (DMF) (5 mL) at 0 °C and stirred at room temperature for 40 min. Then, C11-R (1.00 g, 0.71 mmol) dissolved in 1,2-dichloroethane (30 mL) was added to the mixture and stirred at 78 °C overnight. The mixture was cooled to room temperature and extracted with dichloromethane. The combined organic extracts were washed with water for three times, dried with anhydrous $MgSO_4$, filtered, and the solvent was removed under reduced pressure. The obtained crude product was further purified by column chromatography on silica gel. The eluent is PE: DCM (3:7, v:v). The final product C11-CHO was obtained as a bright yellow

solid (0.86 g, 81.8%).

SMA-C11: Under nitrogen protection, C11-CHO (640 mg, 0.45 mmol), 2-(5-bromo-3-oxo-2,3-dihydro-1H-inden-1-ylidene)malononitrile (365 mg, 1.35 mmol) and chloroform (50 mL) was added to 100 mL two-necked round bottom flask. After the reaction mixture was stirred at room temperature for 30 min, pyridine (0.5 mL) was then added. The reaction mixture was allowed to stir at 60 ºC overnight. After removal of solvent of reaction mixture, which was purified by column chromatography on silica gel with PE: DCM (6:4) as an eluent to afford SMA-C11 as a dark solid (759 mg, 85.0 %).^{1}H NMR (600 MHz, $CDCl_3$) δ 9.18 (s, 2H), 8.56 (d, J = 8.4 Hz, 2H), 8.03 (d, J = 1.9 Hz, 2H), 7.86 (d, J = 1.9 Hz, 2H), 4.77 (d, J = 7.8 Hz, 4H), 3.24-3.21 (m, 4H), 2.13-2.11 (m, 2H), 1.88- 1.86 (m, 4H), 1.56-1.54 (m, 9H), 1.39-1.37 (m, 4H), 1.29-1.27 (m, 30H), 1.21-1.19 (m, 4H), 1.17-1.10 (m, 18H), 1.05-1.00 (m, 36H), 0.98-83 (m, 10H), 0.83-0.77 (m, 18H).MS (MALDI-TOF) *m/z*: $[M + H]^+$ calcd for $C_{114}H_{152}Br_2N_8O_2S_5$, 1984.90, found: 1984.5.

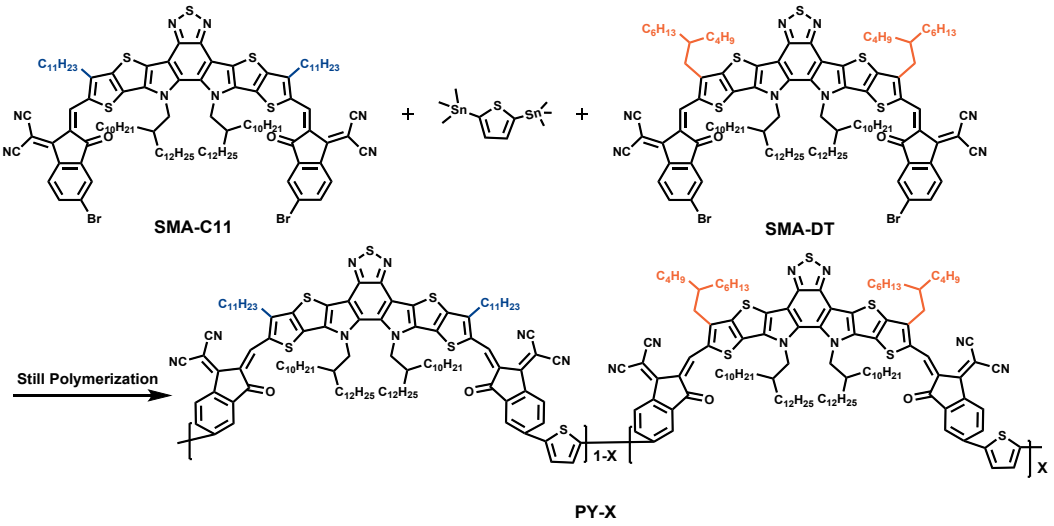

Scheme S2. The synthetic route of PY-X.

PY-X: Under nitrogen protection, SMA-C11, SMA-DT and 2,5-bis(trimethylstannyl)thiophene (20.5 mg, 0.05 mmol), $Pd_2(dba)_3$ (1.6 mg) and $P(o\text{-}tol)_3$ (2.2 mg) and degassed toluene were added to 10 mL round bottom flask. After the reaction mixture was stirred at 110 °C for 4.5 h. Then the mixture was poured into methanol (20 mL) and precipitation occurred. Then the resulting mixture was filtered. The obtained crude polymer was dissolved in warm chloroform and then the solution was quickly filtered through a pre-prepared wet silica gel column with chloroform (100~200 mesh). The collected chloroform solution was concentrated and precipitated in methanol to get PY-X as a dark solid.

PY-C11: The starting materials are SMA-C11 (99.3 mg, 0.05 mmol) and SMA-DT (0 mg, 0 mmol). The final

product PY-C11 was obtained as a dark solid (70.7 mg, 74.1 %). (GPC: M_n=9.3 kDa, M_w=18.6 kDa; PDI=2.00.)

PY-91: The starting materials are SMA-C11 (89.3 mg, 0.045 mmol) and SMA-DT (10.1 mg, 0.005 mmol). The final product PY-91 was obtained as a dark solid (73.4 mg, 76.7 %). (GPC: M_n=8.6 kDa, Mw=17.2 kDa; PDI=2.01.)

PY-82: The starting materials are SMA-C11 (76.4 mg, 0.04 mmol) and SMA-DT (19.4 mg, 0.01 mmol). The final product PY-82 was obtained as a dark solid (69.2 mg, 72.2 %). (GPC: Mn=8.9 kDa, M_w=20.7 kDa; PDI=2.32.)

PY-73: The starting materials are SMA-C11 (66.89 mg, 0.035 mmol) and SMA-DT (29.1 mg, 0.015 mmol). The final product PY-73 was obtained as a dark solid (71.2 mg, 74.2 %). (GPC: M_n=10.7 kDa, M_w=21.0 kDa; PDI=1.97)

PY-DT: The starting materials are SMA-C11 (0 mg, 0 mmol) and SMA-DT (100.6 mg, 0.05 mmol). The final product PY-DT was obtained as a dark solid (72.2 mg, 74.6 %). (GPC: M_n=7.2 kDa, M_w=14.3 kDa; PDI=1.98)

Materials Characterizations: The nuclear magnetic resonance (NMR) spectra were recorded on a Bruker Avance III 600 MHz spectrometer with deuterated chloroform ($CDCl_3$) and trimethylsilane (TMS) as the solvent and internal reference, respectively. The mass spectra were measured using Bruker Daltonics Biflex III MALDI-TOF Analyzer in the MALDI mode. The high temperature gel permeation chromatography (HT-GPC) spectra were measured using PL-GPC 220 Analyzer in 1,2,4-trichlorobenzene at 150 ºC.

Measurements: The UV-visible near infrared absorption spectra were measured using a Shimadzu (model UV-3700) Ultraviolet Visible Near Infrared Spectrophotometer. Cyclic voltammetry (CV) measurements were performed on a CHI660E electrochemical workstation in a three-electrode cell in anhydrous acetonitrile solvents solution of Bu_4NPF_6 (0.1 M) with a scan rate of 50 mV/s at room temperature under argon. An Ag/Ag^+ wire, two platinum wires were used as the reference electrode, counter electrode, and working electrode, respectively. The materials to be tested in chloroform solution were dried on the surface of the working electrode. The potential of Ag/Ag^+ reference electrode was internally calibrated by using ferrocene/ ferrocenium (Fc/Fc^+) as the redox couple. Atomic force microscopy (AFM) were performed on a Dimension Icon AFM (Bruker) in a tapping mode.

Device fabrication: All polymer solar cells (all-PSCs) were fabricated with a conventional architecture of indium tin oxide (ITO)/poly(3,4-ethylenedioxythiophene):polystyrene sulfonate (PEDOT:PSS)/active-layer/PNDIT-F3N/Ag. The ITO-coated glass substrates were sequentially cleaned in detergent, deionized water, acetone and isopropyl alcohol for 15 min each at room temperature and then dried in oven overnight. Before use, ITO-coated substrates were treated by plasma for 2 min. A 40-nm-thick PEDOT:PSS layer was first spin-cast on the top of the ITO substrates at 4000 rpm for 30 s and then annealed on a hotplate at 150 °C for 15 min under ambient conditions. The blend solutions were prepared by dissolving PM6 and PY-X in chloroform solvent with a weight ratio of 1:1. The total concentration of all active layer solutions was maintained at 13 mg ml^{-1}. 1-chloronaphthalene (CN) was used as additive. The optimized content of CN is 1% (vol%). The active layers were obtained by spin-coating the blend solutions at a spin-coating rate of 2500 rpm for 30 s on the top of PEDOT:PSS with an optimal thickness of 120 nm, and then were thermally annealed at 80 °C for 8 min in a N_2-filled glove box. A thin layer (~5 nm) of PNDIT-F3N was spin-cast on the top of the active layer at a spin-coating rate of 2000 rpm for 30s. The PNDIT-F3N solution was prepared by dissolving PNDIT-F3N in mixed solvent (methanol:acetic acid is 200:1) with a concentration of 0.5 mg/ml. Finally, a 120-nm-thick Ag electrode was thermally deposited under vacuum conditions of 2×10^{-4} Pa. A photon mask with a well-defined aperture size was used in the cell measurement to reduce the light piping and internal-scattering-induced edge effect to access J_{sc} more accurately. The active area of the device is 5.12 mm^2, and the mask area is 3.152 mm^2. The solar-cell performance test used an Air Mass 1.5 Global (AM 1.5 G) solar simulator (SS-F5-3A, Enlitech) with an irradiation intensity of 100 mW cm^{-2}, which was measured by a calibrated silicon solar cell (SRC2020, Enlitech). The *J-V* curves were measured along the forward scan direction from -0.5 to 1 V, with a scan step of 50 mV and a dwell time of 10 ms, using a Keithley 2400 Source Measure Unit. EQE spectra were measured by using a solar-cell spectral-response measurement system (QE-R3011, Enlitech).

Photostability test: Photostability of glass-encapsulated PM6:PY-X devices were tested under Maximum Power Point Tracking with 1-sun illumination (white LED lamp) at the temperature of 40 °C and the ambient humidity. At the beginning of the test, the bias voltage is usually set at 0 V and the disturbance step is 0.01 V. As the test goes on, the bias voltage setting and step can be changed automatically, until the bias voltage approaches to the maximum power point voltage V_{max}.

Space-charge-limited current measurement: The charge transport properties of the neat film and blend film were investigated by a space-charge-limited current method. The hole-only devices were fabricated with a configuration of ITO/PEDOT:PSS/PM6:PY-X/Ag, while the electron-only devices were fabricated with a structure of ITO/ZnO/PM6:PY-X or PY-X /PNDIT-F3N-Br/Ag. The mobility was determined by fitting the dark current with the Mott-Gurney law described as $J=9\varepsilon_0\varepsilon_r\mu V^2/8L^3$, where J is the current density, ε_0 is the permittivity of free space, ε_r is the permittivity of the active layer, μ is the hole mobility (μ_h) or electron mobility (μ_e), V is the effective voltage ($V=V_{appl}-V_{bi}-V_r$, where V_{appl} is the applied voltage and V_{bi} is the built-in potential, and V_r is the voltage loss on series resistance) and L is the film thickness of the neat film or blend film.

Grazing Incidence Wide-Angle X-ray Scattering (GIWAXS):

GIWAXS measurements were conducted on a Xenocs-SAXS/WAXS system with an X-ray wavelength of 1.5418 Å. Pilatus3 R 300K was used as a 2D detector. Samples were prepared on Si/PEDOT:PSS substrates under the same conditions as those used for device fabrication.

EL: The EL spectra were measured using a Shamrock SR-303i spectrometer from Andor Tech with a Newton EM-CCD Si and an iDus InGaAs array detector at -70 °C. The electrical bias used for the EL measurement was applied on the devices using a Keithley 2400 SourceMeter. The emission spectra of the OSCs were recorded with the injection currents smaller or similar to the J_{sc} of the device under 1 sun illumination, and the spectra were corrected for the optical losses in the measurement setup using a calibrated halogen lamp (HL-3P-CAL, Ocean. Optics Germany GmbH).

EQE_{EL}: EQE_{EL} values were obtained from an in-house-built system including a Hamamatsu silicon photodiode 1010B, a Keithley 2400 SourceMeter to provide voltage and inject current, and a Keithley 6482 Picoammeter to measure the emitted light intensity.

Determination of V_{oc}^{rad} :

The E_{loss} terms in the organic solar cells studied in this work are evaluated using the measurement of the sensitive EQE spectra for the determination of J_0^{rad} i.e. the radiative recombination limit for the dark saturation current,

$$J_{0,rad} = q\int BB(E)EQE_{PV}(E)dE \quad \text{eq. S1}$$

where (E) is the blackbody emission photo flux and E is the photon energy.

V_{oc}^{rad}, the radiative limit for the V_{oc} of the solar cell (with 100% EQE_{EL}), is determined using the following equation.

$$V_{oc} \approx \frac{kT}{q}\ln\left(\frac{J_{ph}}{J_{0,rad}}\right) \quad \text{eq. S2}$$

where k is the Boltzmann constant, q is the elementary charge, and J_{ph} is the photocurrent density in the solar cell under an open-circuit voltage (assumed to be equivalent to the short-circuit current density).

Highly sensitive EQE (sEQE): Highly sensitive EQE (sEQE) measurements were performed using a halogen lamp, a monochromator (Newport cornerstone cs260), an optical chopper, a pre current amplifier (Stanford Instrument SR-570), a lock-in amplifier (Stanford Instrument SR 830), and a set of long pass filters.

Transient absorption spectroscopy (TAS): The TAS measurements were conducted using a Yb:KGW laser (Pharos, Light Conversion). The wavelength of fundamental output was at ~1030 nm. We used a home-built noncollinear optical parametric amplifier to generate the pump beam. The pump beam was filtered by a bandpass filter (FB800-40, thorlabs) to selectively excite the acceptors. The pump density was kept below 2μJ/cm^2. The probe beam was supercontinuum generated by focusing a small fraction of the fundamental 1030 beam to a 5 mm sapphire plate for detection. The pump and probe beams were compressed by chirp mirrors and wedge pairs. The probe beam was split into two beams (probe and reference) for double-line detection. The probe and reference beams were then routed to a double-line Si camera (S14417, Hamamatsu) for visible detection mounted on a monochrometor (Acton 2358, Princeton Instrument). Pulse-to-pulse spectral analysis was conducted at the rate of 50 kHz enabled by a homebuilt field-programmable gate array (FPGA) control board. The noise level (ΔT/T) was better than 10^{-5} (std) after averaging 25k pump-on and pump-off shots for each data point. The samples were kept in nitrogen atmosphere during the measurement to prevent photon induced degradation.

Flexible OSC fabrication: The flexible OSCs were fabricated by using AgNWs as the cathode electrode on the top of a 30 μm-thick PET substrate with the device structure of PET/AgNWs/ZnO/active layers/MoO_3/Ag. PET/AgNWs electrode was prepared according to the previously reported work.[3] In details, the pre-cleaned

30 μm-thick PET substrate was attached to PDMS-coated glass substrates in advance. The specific concentration AgNWs dispersion (Gu's New Material) solution was spin cast on the top of PET substrate and then annealed at 100 °C for 10 min. After that, the ZnO sol-gel was repeatedly spin cast onto a patterned PET/AgNWs electrode to form a dense ZnO layer with the following thermal annealing at 150 °C for 30 min. After spin coating the active layers, a 10-nm-thick MoO_3, and a 80-nm-thick Ag are sequentially deposited to fabricate the whole fabrication of the flexible OSCs.

Bending test of the flexibleOSCs: To test the mechanical performance ofthe flexible devices, an auto cyclic mechanical bending test system was designed in the glove box. The system main consisted of the two contact fixtures. One of the fixtures could be moved reciprocally at a constant speed and the other was fixed. All cyclic mechanical bending tests of flexible OSCs were conducted in a nitrogen atmosphere.

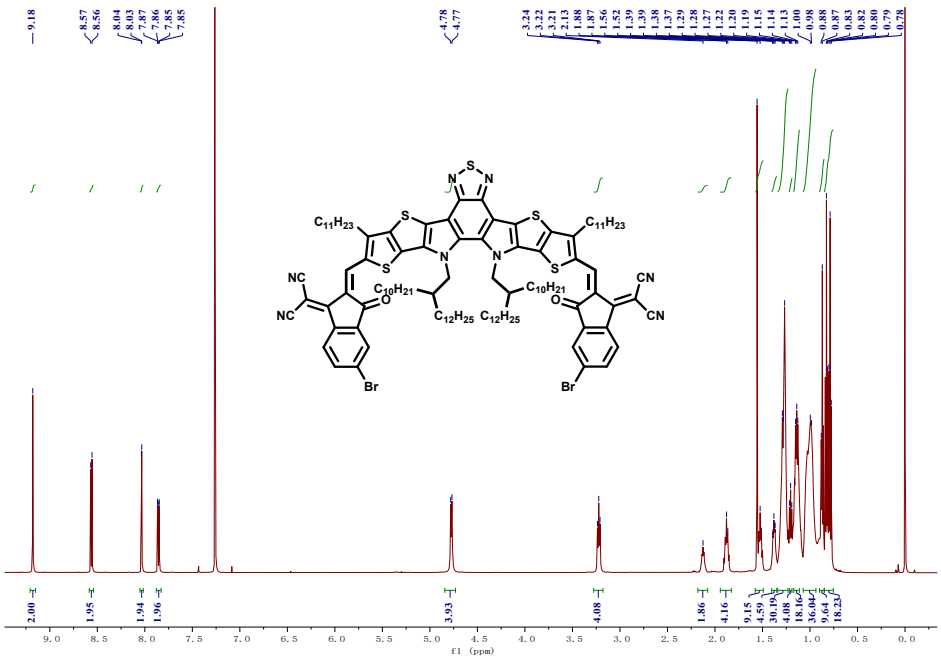

Fig. S1 ^{1}H NMR spectrum of SMA-C11.

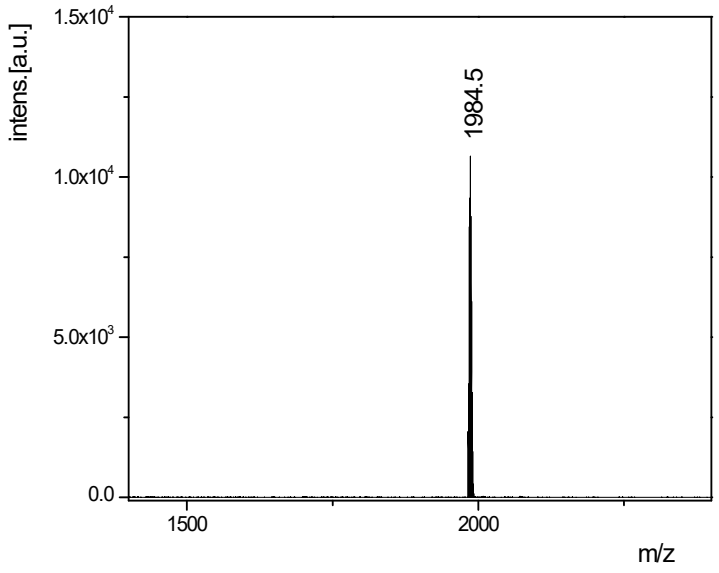

Fig. S2 MS (MALDI-TOF) spectrum of SMA-C11.

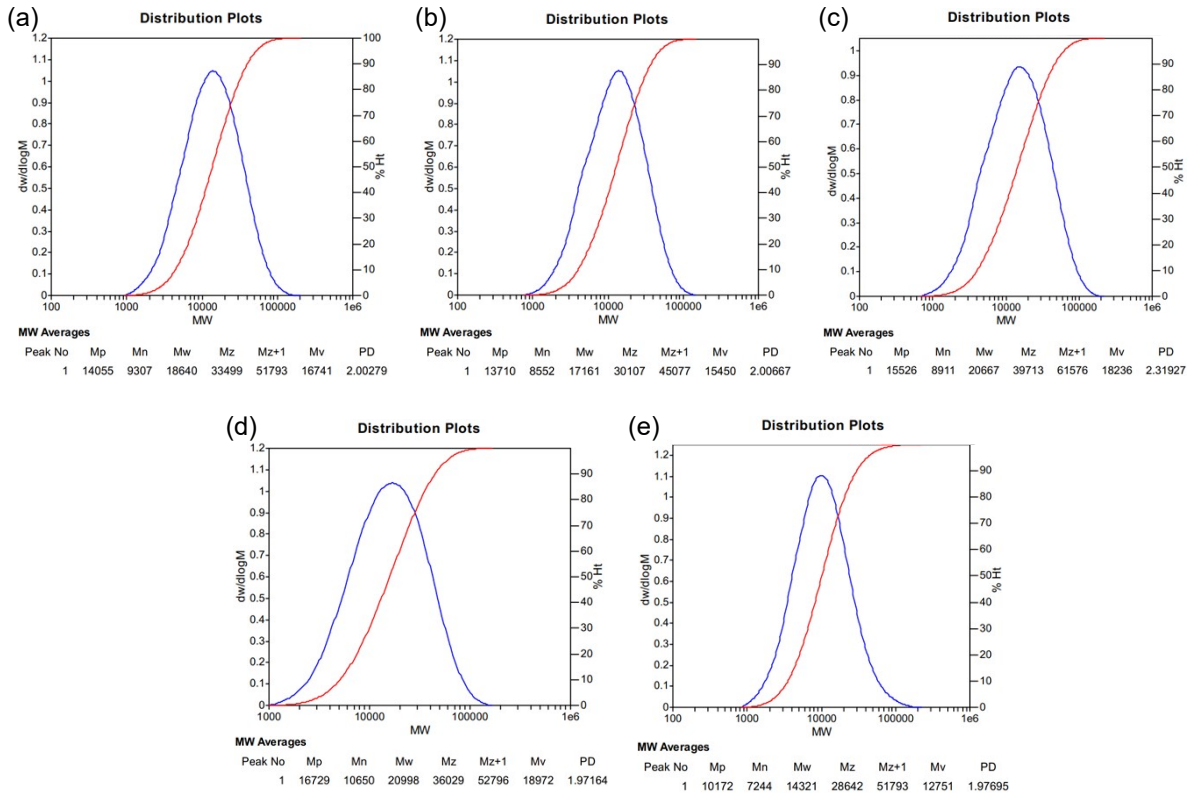

Fig. S3 HT-GPC measurements of (a) PY-C11, (b) PY-91, (c) PY-82, (d) PY-73, and (e) PY-DT.

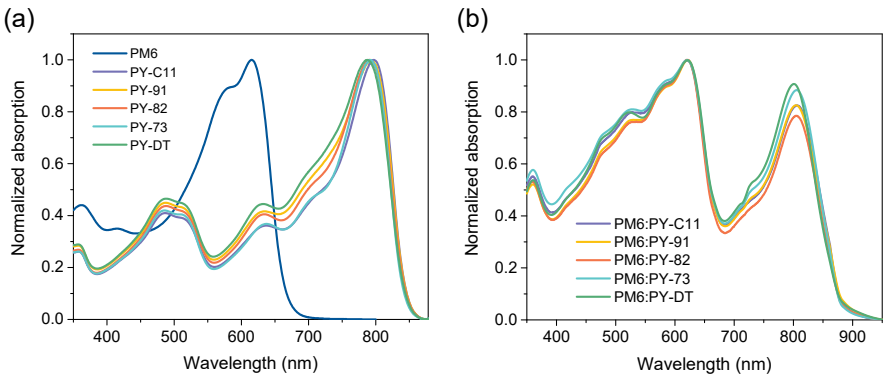

Fig. S4 Normalized absorption spectra of (a) PM6, PY-C11, PY-91, PY-82, PY-73, and PY-DT in diluted chloroform solution and (b) PM6:PY-X films.

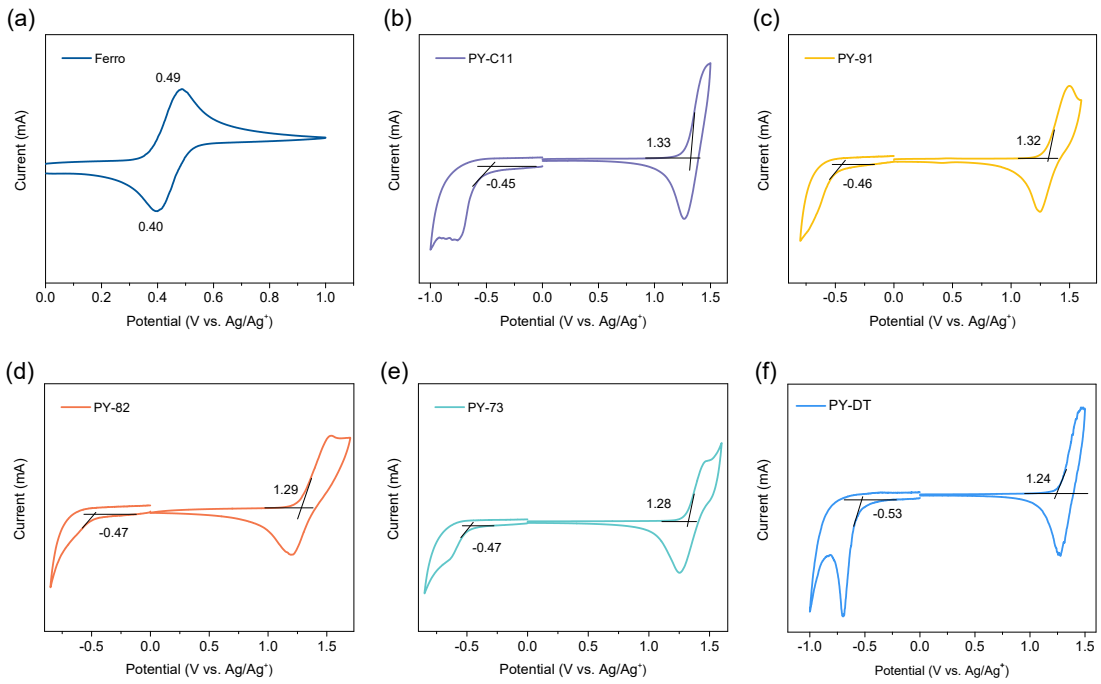

Fig. S5 Cyclic voltammetry measurements of (a) PM6, (b) PY-C11, (c) PY-91, (d) PY-82, (e) PY-73, and (f) PY-DT.

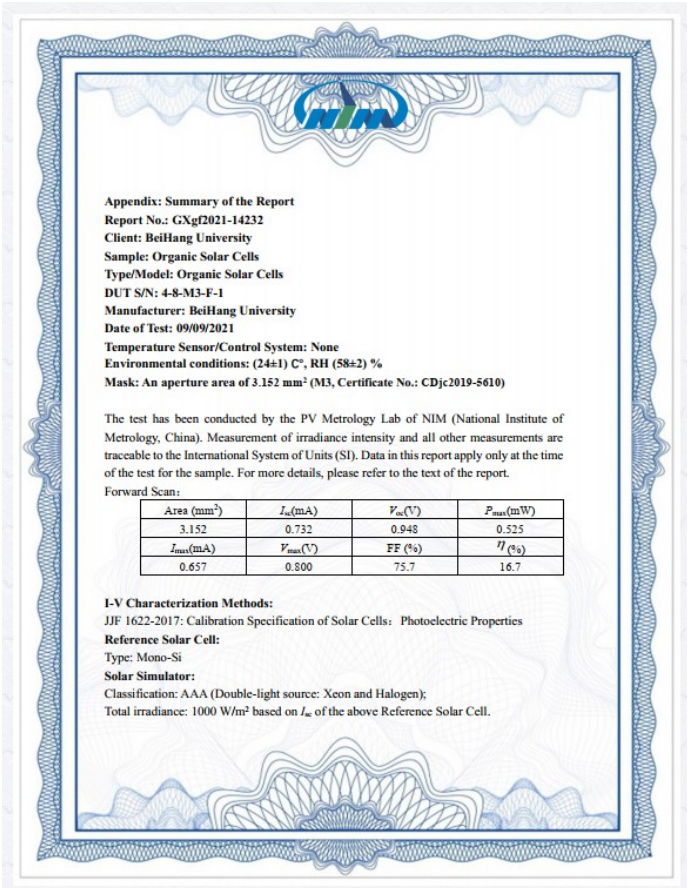

Appendix: Summary of the Report
Report No.: GXgf2021-14232
Client: BeiHang University
Sample: Organic Solar Cells
Type/Model: Organic Solar Cells
DUT S/N: 4-8-M3-F-1
Manufacturer: BeiHang University
Date of Test: 09/09/2021
Temperature Sensor/Control System: None
Environmental conditions: (24±1) C°, RH (58±2) %
Mask: An aperture area of 3.152 mm² (M3, Certificate No.: CDjc2019-5610)

The test has been conducted by the PV Metrology Lab of NIM (National Institute of Metrology, China). Measurement of irradiance intensity and all other measurements are traceable to the International System of Units (SI). Data in this report apply only at the time of the test for the sample. For more details, please refer to the text of the report.

Forward Scan:

Area (mm^2)	I_{sc}(mA)	V_{oc}(V)	P_{max}(mW)
3.152	0.732	0.948	0.525
I_{max}(mA)	V_{max}(V)	FF (%)	η(%)
0.657	0.800	75.7	16.7

I-V Characterization Methods:
JJF 1622-2017: Calibration Specification of Solar Cells: Photoelectric Properties
Reference Solar Cell:
Type: Mono-Si
Solar Simulator:
Classification: AAA (Double-light source: Xeon and Halogen);
Total irradiance: 1000 W/m² based on I_{sc} of the above Reference Solar Cell.

Fig. S6 Report of certified efficiency of PM6:PY-82 device from National Institute of Metrology, China.

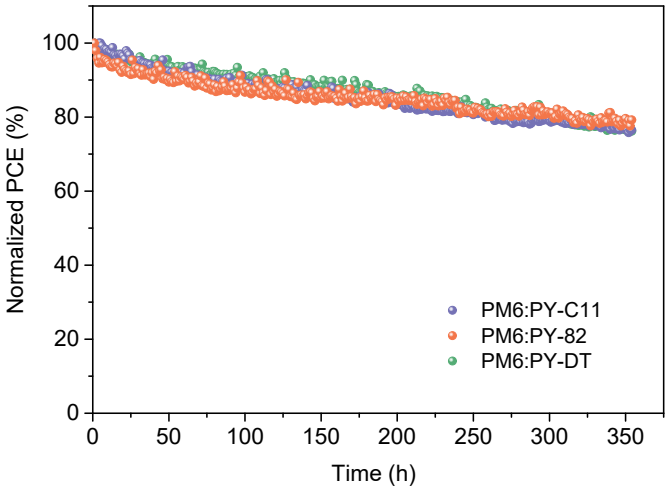

Fig. S7 Photostability of all-PSCs measured using maximum power point (MPP) tracking methods.

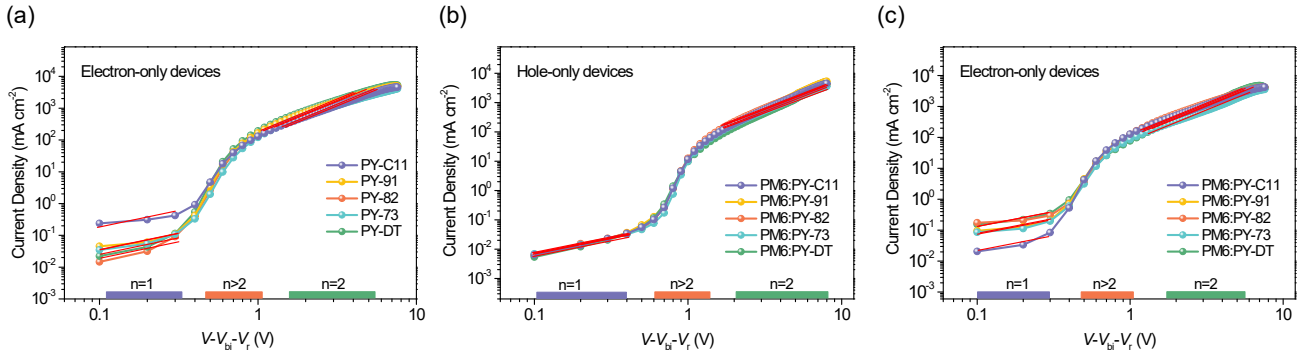

Fig. S8 SCLC curves of (a) electron-only devices based on PY-X neat films, (b) hole-only devices based on PM6:PY-X blend films, and (c) electron-only devices based on PM6:PY-X blend films.

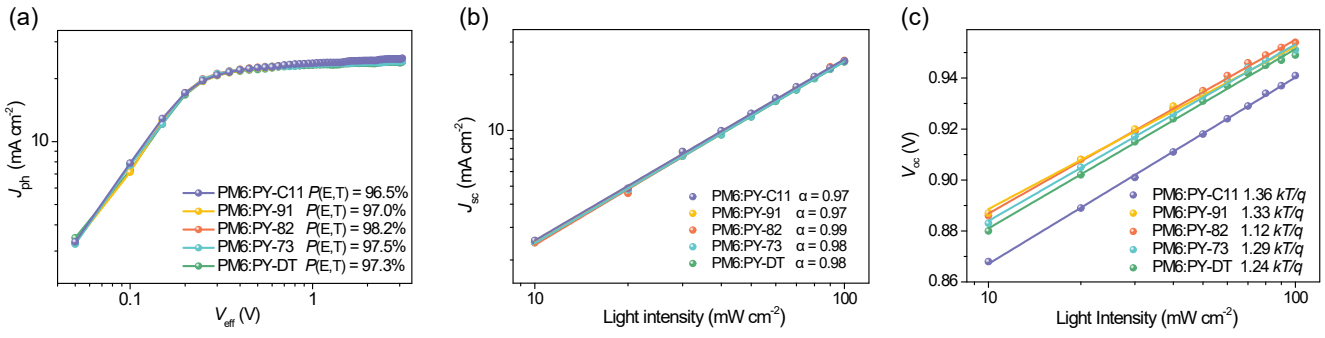

Fig. S9 (a) V_{oc} *versus* P_{light} intensity characteristics of all-PSCs based on PM6:PY-X. (b) J_{sc} *versus* P_{light} intensity characteristics of all-PSCs based on PM6:PY-X. (c) J_{ph} *versus* V_{eff} characteristics of all-PSCs based on PM6:PY-X.

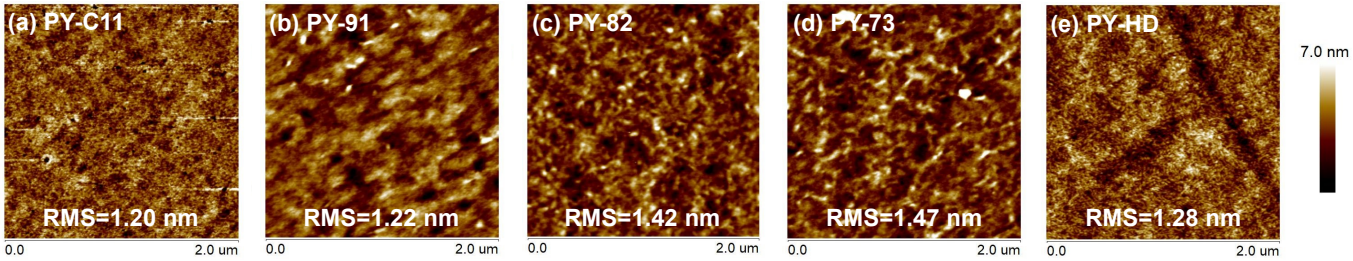

Fig. S10 AFM phase images (2 μm×2 μm) of (a) PY-C11, (b) PY-91, (c) PY-82, (d) PY-73, and (e) PY-DT neat films.

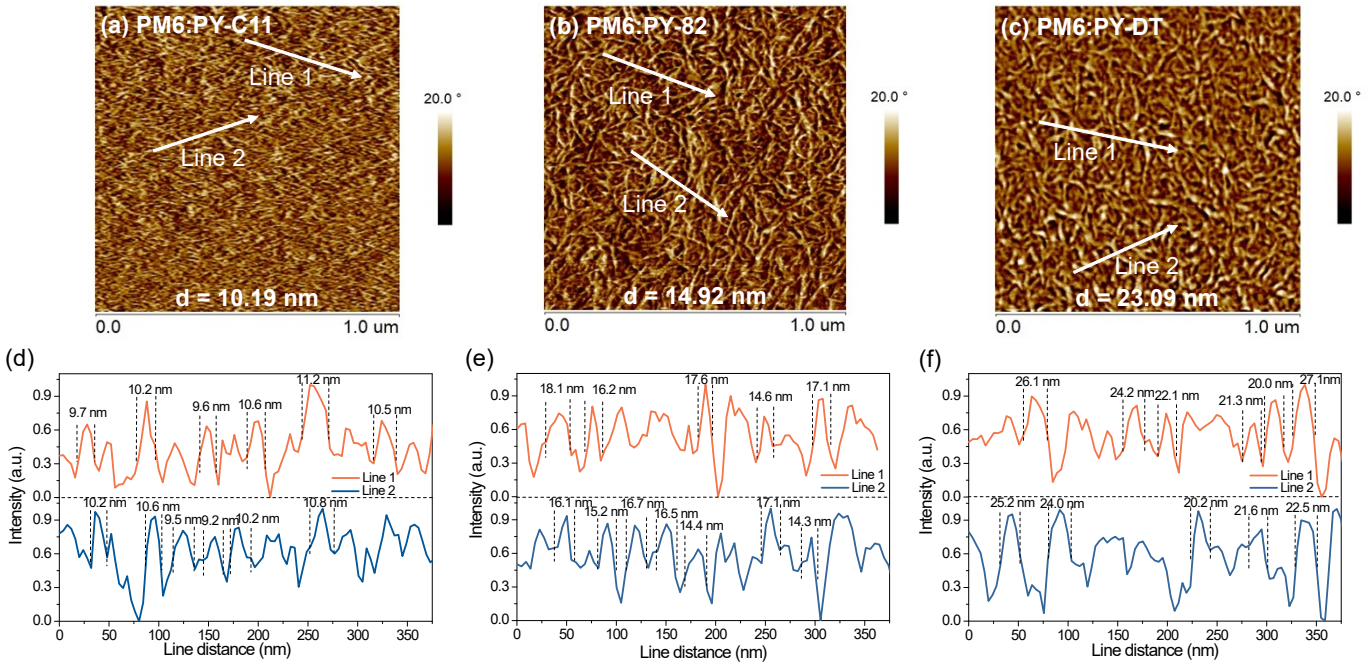

Fig. S11 AFM phase images (1 μm×1 μm) of (a) PM6:PY-C11, (b) PM6:PY-82, (c) PM6:PY-DT films, and the corresponding line profiles of (d) PM6:PY-C11, (e) PM6:PY-82, and (f) PM6:PY-DT blend films to obtain the FWHMs of cross-sections though AFM images.

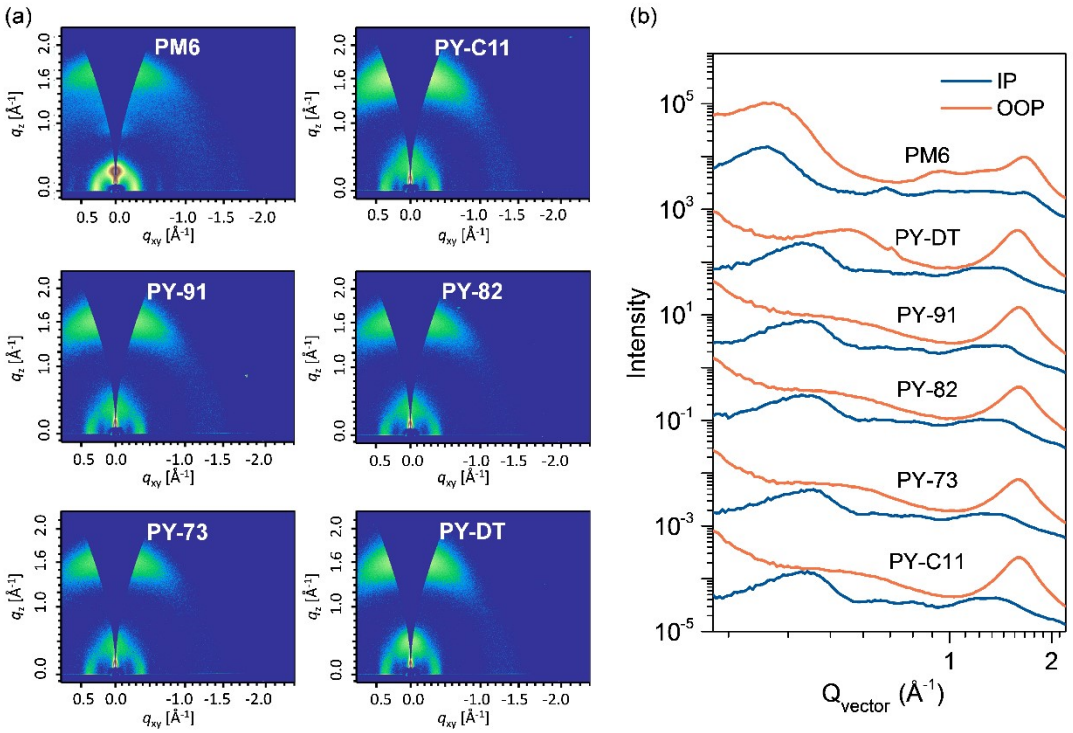

Fig. S12 (a) 2D GIWAXS profiles of PM6, PY-C11, PY-91, PY-82, PY-73, and PY-DT neat films and (b) the corresponding IP and OOP line cuts.

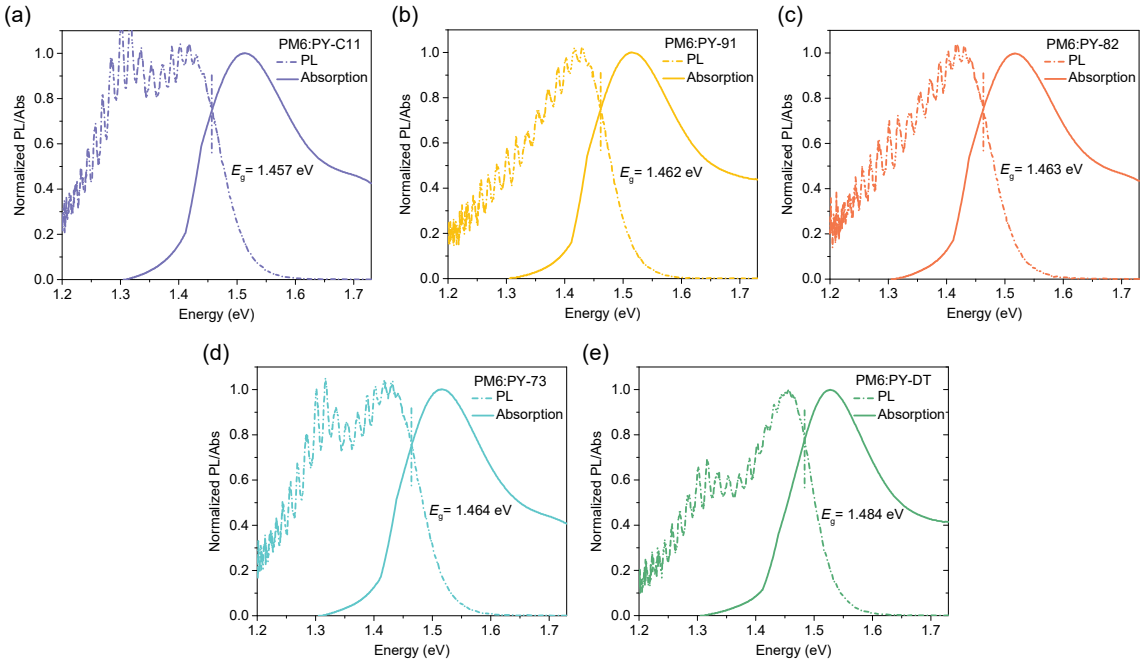

Fig. S13 Normalized absorption and photoluminescence spectra of (a) PM6:PY-C11, (b) PM6:PY-91, (c) PM6:PY-82, (d) PM6:PY-73, and (e) PM6:PY-DT films.

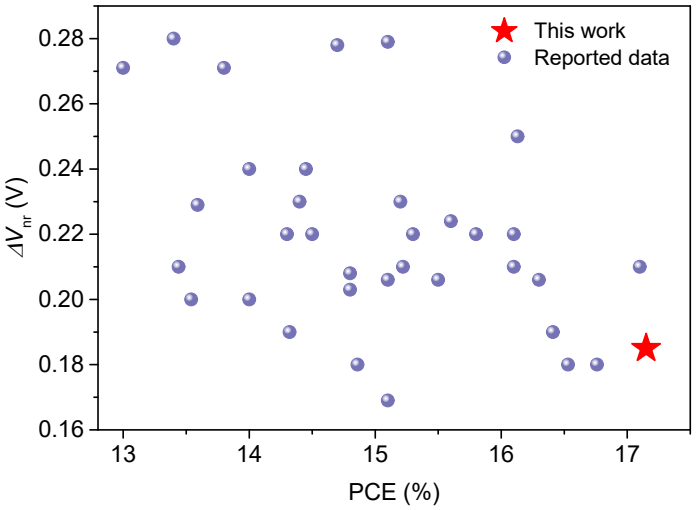

Fig. S14 Comparison of our work with reported PCE and V_{loss} values of binary all-PSCs.

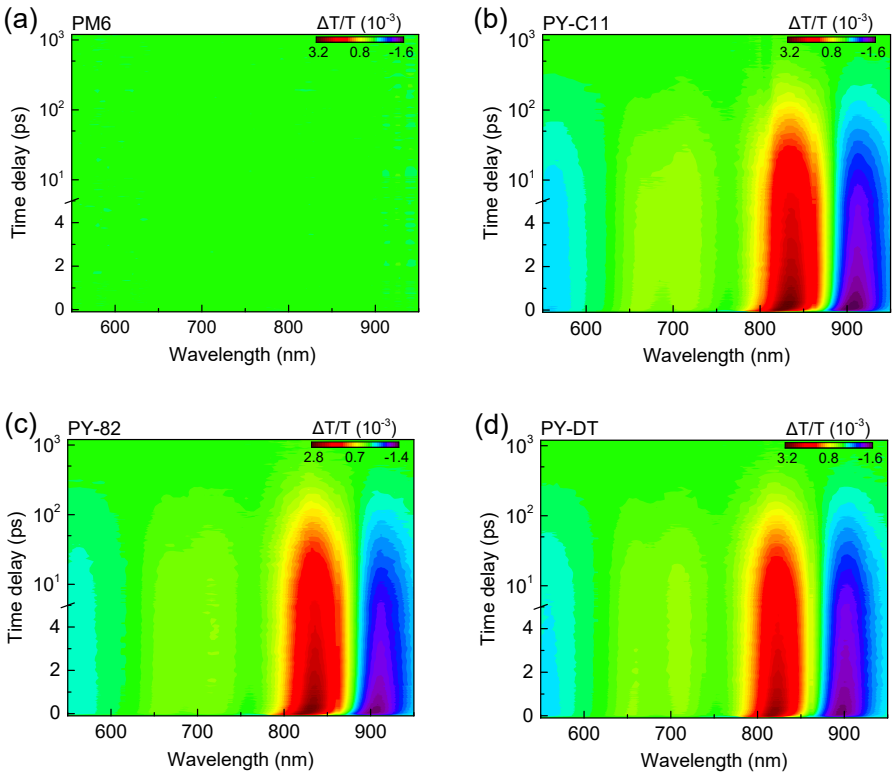

Fig. S15 Color map of the TA data recorded from the neat films of (a) PM6, (b) PY-C11, (c) PY-82, and (d) PY-DT with pump light at 800 nm.

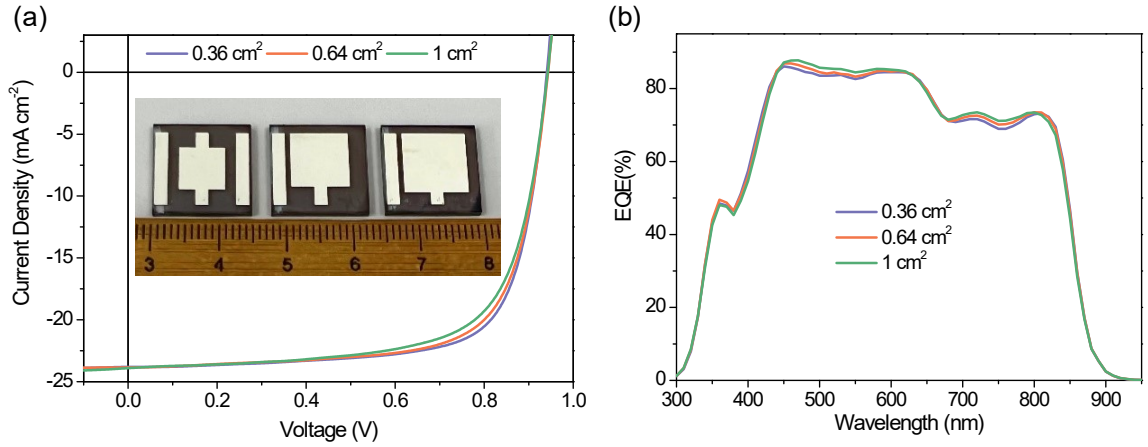

Fig. S16 (a) *J-V* characteristics and (b) the corresponding EQE spectra of all-PSCs based on PM6:PY-82 with different active areas. The inset is a photograph of the real large-area devices with differet active area.

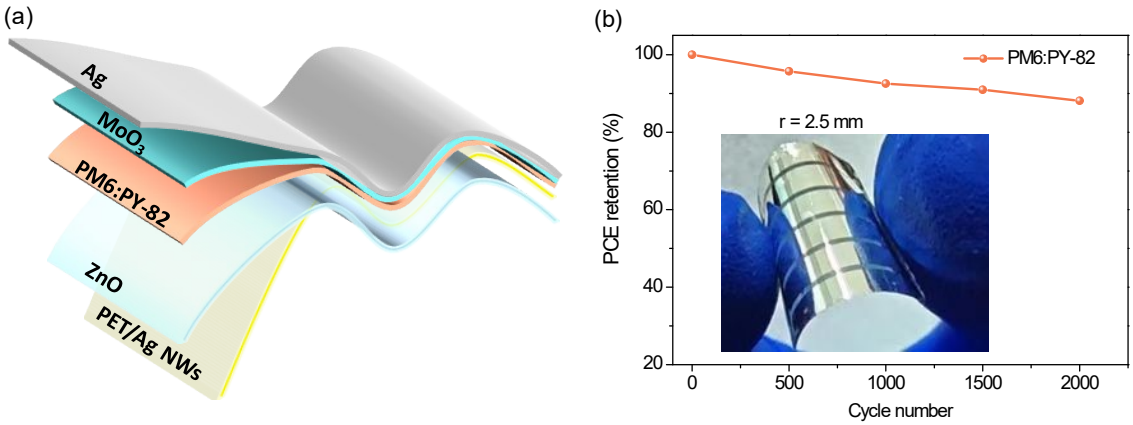

Fig. S17 (a) Device architecture for flexible OSCs. (b) PCE retention of the flexible OSCs measured after bending with different cycle numbers at a bending radius of 2.5 mm. The inset is a photograph of the real flexible device.

Supplementary Tables

Table S1. The hole and electron mobility of PY-X neat films and PM6:PY-X blend films.

Active layer	Hole mobility [10^{-4} cm^2 V^{-1} s^{-1}]	Electron mobility[b] [10^{-4} cm^2 V^{-1} s^{-1}]	μ_h/μ_e
PY-C11	/	5.12±0.14 (83±5 nm)	/
PY-91	/	5.33±0.18 (88±5 nm)	/
PY-82	/	5.21±0.16 (90±5 nm)	/
PY-73	/	5.07±0.14 (99±5 nm)	/
PY-DT	/	5.20±0.19 (102±5 nm)	/
PM6:PY-C11	3.70±0.25 (133±12 nm)[a]	3.26±0.18 (103±12 nm)	1.14
PM6:PY-91	3.66±0.19 (128±14 nm)	3.27±0.24 (108±13 nm)	1.12
PM6:PY-82	3.72±0.21 (122±13 nm)	3.47±0.17 (114±12 nm)	1.07
PM6:PY-73	3.74±0.18 (134±16 nm)	3.42±0.22 (127±10 nm)	1.09
PM6:PY-DT	3.65±0.26 (147±11 nm)	3.32±0.26 (125±11 nm)	1.10

[a]The thickness of the devices

[b]The average results are obtained from 5 different devices

Table S2. Detailed GIWAXS data of PY-X neat films.

Materials	(100) peak				(010) peak			
	q [$Å^{-1}$]	d-spacing [Å]	FWHM [$Å^{-1}$]	CCL [Å]	*q* [$Å^{-1}$]	d-spacing [Å]	FWHM [$Å^{-1}$]	CCL [Å]
PM6	0.29	21.67	0.089	62.83	1.67	3.76	0.236	23.69
PY-C11	0.38	16.53	0.152	36.79	1.60	3.93	0.318	17.59
PY-91	0.38	16.53	0.180	31.07	1.60	3.94	0.318	17.59
PY-82	0.39	16.11	0.155	36.08	1.59	3.95	0.327	17.10
PY-73	0.39	16.11	0.152	36.79	1.58	3.96	0.332	16.84
PY-DT	0.39	16.11	0.152	36.79	1.58	3.97	0.319	17.53

Table S3. Detailed GIWAXS data of PM6:PY-X blend films.

Blends	(100) peak				(010) peak			
	q [$Å^{-1}$]	d-spacing [Å]	FWHM [$Å^{-1}$]	CCL [Å]	*q* [$Å^{-1}$]	d-spacing [Å]	FWHM [$Å^{-1}$]	CCL [Å]
PM6:PY-C11	0.29	21.67	0.093	60.13	1.62	3.88	0.366	15.28
PM6:PY-91	0.29	21.67	0.090	62.13	1.62	3.88	0.371	15.07
PM6:PY-82	0.30	20.94	0.096	58.25	1.62	3.88	0.381	14.68
PM6:PY-73	0.30	20.94	0.093	60.13	1.62	3.88	0.382	14.64
PM6:PY-DT	0.30	20.94	0.105	53.26	1.60	3.93	0.390	14.34

Table S4. The device parameters of all-PSCs based on based on PM6:PY-82 with different active areas.

Device Area (cm^2)	V_{oc} (V)	J_{sc} (mA cm^{-2})	FF (%)	PCE[a] (%)
0.36	0.947 (0.946±0.001)	23.77 (23.51±0.22)	74.1 (73.4±0.5)	16.68 (16.45±0.22)
0.64	0.948 (0.947±0.002)	23.85 (23.60±0.25)	72.2 (71.7±0.4)	16.31 (16.08±0.25)
1	0.947(0.946±0.001)	23.87 (23.60±0.21)	69.3 (68.8±0.6)	15.67 (15.39±0.26)

[a]The average results are obtained from 10 different devices.

Table S5. Comparison of our results with reported binary all-PSCs with PCEs over 13%.

All-Polymer Systems	V_{oc} (V)	J_{sc} (mA cm^{-2})	FF (%)	PCE (%)	E_{loss} (eV)	ΔE_{nr} (eV)	References
PM6:PY-82	**0.950**	**23.82**	**75.8**	**17.15**	**0.513**	**0.185**	**This work**
PBDB-T:PZT-γ	0.896	24.7	71.3	15.8	0.51	0.22	4
PBDB-T:PZT	0.909	23.2	68.6	14.5	0.52	0.22	4
PM6:PYT_M	0.93	21.78	66.33	13.44	0.528	0.210	5
PBDB-T:PJ1	0.9	22.3	70	14.4	0.51	/	6
PM6:L14	0.96	20.6	72.1	14.3	0.53	0.22	7
PBDB-T:PF5-Y5	0.946	20.65	74	14.45	0.57	0.24	8
PM6:PY-IT	0.933	22.3	72.3	15.05	0.47	/	9
PTzBI-oF:PFA1	0.87	23.96	72.67	15.11	/	/	10
PTzBI-oF:PS1	0.92	22.47	66.7	13.8	/	/	11
PBDB-T:PFY-0Se	0.904	20.9	68.8	13.0	0.601	0.271	12
PBDB-T:PFY-1Se	0.894	21.2	72.9	13.8	0.609	0.271	12
PBDB-T:PFY-2Se	0.875	23.4	72.0	14.7	0.579	0.278	12
PBDB-T:PFY-3Se	0.871	23.6	73.7	15.1	0.578	0.279	12
PBDB-T:PYN-BDTF	0.86	22.28	69.0	13.22	/	/	13
PBDB-T:PYTT1	0.93	20.66	70.35	13.54	0.57	0.20	14
PBDB-T: PYTT2	0.91	22.00	71.53	14.32	0.61	0.19	14
PM6:PYF-T	0.891	23.1	68.0	14.0	0.53	0.24	15
PM6:PYF-T-o	0.901	23.3	72.4	15.2	0.52	0.23	15
PM6:PYF-T-m	0.949	4.60	32.7	1.40	0.52	0.20	15
PM6: PY2F-T	0.86	24.27	72.62	15.22	0.52	0.21	16
PBDB-T:PS-Se	0.874	23.27	68.0	13.83	/	/	17
PBDB-T: PN-Se	0.907	24.82	71.8	16.1	/	/	17
PM6:PY2S-H	0.941	22.3	70.7	14.8	0.514	0.203	18
PM6:PY2S-F	0.920	23.3	70.5	15.1	0.510	0.206	18
PM6:PY2Se-F	0.885	24.4	72.2	15.6	0.530	0.224	18
PM6:PY2Se-Cl	0.884	24.5	74.3	16.1	0.533	0.220	18

JD40:PJTVT	0.89	23.75	76.40	16.13	0.57	0.25	18
PBDB-T:PY5-BTZ	0.922	22.61	71.1	14.82	/	/	19
PM6:PYT-2S	0.941	22.3	70.7	14.8	0.516	0.208	20
PM6:PYT-1S1Se	0.926	24.1	73.0	16.3	0.502	0.206	20
PM6:PYT-2Se	0.908	23.9	71.4	15.5	0.509	0.206	20
PM6:PY-HD	0.937	24.05	72.8	16.41	0.55	0.19	21
PM6:PY-OD	0.943	23.95	73.2	16.53	0.55	0.18	21
PM6:PY-DT	0.949	23.73	74.4	16.76	0.54	0.18	21
PM6:PY-DH	0.961	21.39	72.3	14.86	0.53	0.18	21
PM6:PYIT	0.93	21.88	73.40	15.00	/	/	22
Q4:PYIT	0.94	21.59	73.90	15.06	/	/	22
P1-co-25%P2: PYFT	0.83	23.51	73.09	14.67	/	/	23
PBDF-NS:PY-IT	0.859	25.24	74.6	16.17	/	/	24
JD40:PA-5	0.87	24.05	76.88	16.11	/	/	25
JD40:PA-6-L	0.92	22.13	72.99	14.81	/	/	25
JD40:PA6-M	0.92	22.42	72.41	14.99	/	/	25
PBDB-T/PYT	0.91	23.07	77.00	16.05%	/	/	26
PBQx-H-TF:PBTIC-γ-TT	0.916	22.88	67.80	14.21	/	/	27
PBDB-T:RRg-C20	0.88	23.54	73.00	15.12	/	/	28
PBDB-T: RRg-C24	0.88	21.67	71.00	13.53	/	/	28
PBDB-T: PYTS-0.0	0.92	22.38	63.00	13.01	/	/	29
PBDB-T: PYTS-0.1	0.92	22.52	68.00	14.19	/	/	29
PBDB-T: PYTS-0.3	0.92	22.91	70.00	14.68	/	/	29
PTzBI-Si:PRiC39	0.90	23.1	69.4	14.40	0.57	0.23	30
PTzBI-Si:PRoC39	0.83	22.1	73.2	13.40	0.63	0.28	30
PM6: PY-IT	0.948	22.31	73.50	15.56	/	/	31
J71:PY-IT	0.914	21.44	68.50	13.43	/	/	31
PBQx-H-T: PBTIC-γ-TSe	0.91	23.49	73.8	15.77	/	/	32
PBDB-T: PYSe-TCl10	0.894	22.84	64.3	13.23	/	/	33
PBDB-T: PYSe-TCl20	0.902	23.08	68.3	14.21	/	/	33
PM6:PY-V-γ	0.912	24.8	75.8	17.1	0.54	0.21	34
PM6:PY-T-γ	0.929	24.1	71.9	16.1	0.55	0.21	34
PM6:PY-2T-γ	0.933	23.4	69.9	15.3	0.56	0.22	34
PBDB-T:PZT-C12	0.928	22.2	63.7	13.1			35
PBDB-T:PZT-C8	0.918	22.8	65.9	13.8			35
PBDB-T:PZT-C1	0.912	23.9	68.5	14.9			35
PBDB-T: PYT	0.902	22.29	67.58	13.59	0.545	0.229	36
PBDB-T: PYT-Tz	0.916	23.00	71.68	15.10	0.508	0.169	36

References

1. J. Yuan, Y. Zhang, L. Zhou, G. Zhang, H.-L. Yip, T.-K. Lau, X. Lu, C. Zhu, H. Peng, P. A. Johnson, M. Leclerc, Y. Cao, J. Ulanski, Y. Li and Y. Zou, *Joule,* 2019, **3**, 1140-1151.
2. A.Hexemer, W. Bras, J. Glossinger, E. Schaible, E. Gann, R. Kirian, A. MacDowell, M. Church, B. Rude and H. Padmore, *J. Phys. Conf. Ser.,* 2010, **247**, 012007.
3. C. Xie, X. Jiang, Q. Zhu, D. Wang, C. Xiao, C. Liu, W. Ma, Q. Chen and W. Li, *Small Methods*, 2021, **5**, 2100481.
4. H. Fu, Y. Li, J. Yu, Z. Wu, Q. Fan, F. Lin, H. Y. Woo, F. Gao, Z. Zhu and A. K. Y. Jen, *J. Am. Chem. Soc.,* 2021, ***143***, 2665.
5. W. Wang, Q. Wu, R. Sun, J. Guo, Y. Wu, M. Shi, W. Yang, H. Li and J. Min, *Joule,* 2020, ***4***, 1070.
6. T. Jia, J. Zhang, W. Zhong, Y. Liang, K. Zhang, S. Dong, L. Ying, F. Liu, X. Wang, F. Huang and Y. Cao, *Nano Energy,* 2020, ***72***, 104718.
7. H. Sun, H. Yu, Y. Shi, J. Yu, Z. Peng, X. Zhang, B. Liu, J. Wang, R. Singh, J. Lee, Y. Li, Z. Wei, Q. Liao, Z. Kan, L. Ye, H. Yan, F. Gao and X. Guo, *Adv. Mater.,* 2020, **32**, 2004183.
8. Q. Fan, Q. An, Y. Lin, Y. Xia, Q. Li, M. Zhang, W. Su, W. Peng, C. Zhang, F. Liu, L. Hou, W. Zhu, D. Yu, M. Xiao, E. Moons, F. Zhang, T. D. Anthopoulos, O. Inganäs and E. Wang, *Energy Environ. Sci.,* 2020, **13**, 5017.
9. Z. Luo, T. Liu, R. Ma, Y. Xiao, L. Zhan, G. Zhang, H. Sun, F. Ni, G. Chai, J. Wang, C. Zhong, Y. Zou, X. Guo, X. Lu, H. Chen, H. Yan and C. Yang, *Adv. Mater.,* 2020, **32**, 2005942.
10. F. Peng, K. An, W. Zhong, Z. Li, L. Ying, N. Li, Z. Huang, C. Zhu, B. Fan, F. Huang and Y. Cao, *ACS Energy Lett.,* 2020, **5**, 3702.
11. C. Zhu, Z. Li, W. Zhong, F. Peng, Z. Zeng, L. Ying, F. Huang and Y. Cao, *Chem. Commun.,* 2021, **57**, 935.
12. Q. Fan, H. Fu, Q. Wu, Z. Wu, F. Lin, Z. Zhu, J. Min, H. Y. Woo and A. K.-Y. Jen, *Angew. Chem. Int. Ed.,* 2021, **60**, 15935.
13. N. Su, R. Ma, G. Li, T. Liu, L.-W. Feng, C. Lin, J. Chen, J. Song, Y. Xiao, J. Qu, X. Lu, V. K. Sangwan, M. C. Hersam, H. Yan, A. Facchetti and T. J. Marks, *ACS Energy Lett.,* 2021, **6**, 728.
14. T. Wang, R. Sun, W. Wang, H. Li, Y. Wu and J. Min, *Chem. Mater.,* 2021, **33**, 761.
15. H. Yu, M. Pan, R. Sun, I. Agunawela, J. Zhang, Y. Li, Z. Qi, H. Han, X. Zou, W. Zhou, S. Chen, J. Y. L. Lai, S. Luo, Z. Luo, D. Zhao, X. Lu, H. Ade, F. Huang, J. Min and H. Yan, *Angew. Chem. Int. Ed.,* 2021,

60, 10137.

16. H. Yu, S. Luo, R. Sun, I. Angunawela, Z. Qi, Z. Peng, W. Zhou, H. Han, R. Wei, M. Pan, A. M. H. Cheung, D. Zhao, J. Zhang, H. Ade, J. Min and H. Yan, *Adv. Funct. Mater.,* 2021, **31**, 2100791.
17. J. Du, K. Hu, J. Zhang, L. Meng, J. Yue, I. Angunawela, H. Yan, S. Qin, X. Kong, Z. Zhang, B. Guan, H. Ade and Y. Li, *Nat. Commun.,* 2021, ***12***, 5264.
18. Q. Fan, H. Fu, Z. Luo, J. Oh, B. Fan, F. Lin, C. Yang and A. K. Y. Jen, *Nano Energy,* 2021, **92**, 106718.
19. L. Zhou, X. Xia, L. Meng, J. Zhang, X. Lu and Y. Li, *Chem. Mater.,* 2021, ***33***, 8212.
20. H. Fu, Q. Fan, W. Gao, J. Oh, Y. Li, F. Lin, F. Qi, C. Yang, T. J. Marks and A. K.-Y. Jen, *Sci. China Chem.*, 2022, **65**, 309-317.
21. Y. Li, J. Song, Y. Dong, H. Jin, J. Xin, S. Wang, Y. Cai, L. Jiang, W. Ma, Z. Tang and Y. Sun, *Adv. Mater.*, 2022, 2110155.
22. C. Liao, Y. Gong, X. Xu, L. Yu, R. Li and Q. Peng, *Chem. Eng. J.*, 2022, **435**, 134862.
23. M. Shao, M. Xu, D. Zhang, Z. Wang, Z. Liu, X. Gao, J. He, Y. Gao, Z. Li SSRN:https://ssrn.com/abstract=4011812
24. X. Li, X. Duan, Z. Liang, L. Yan, Y. Yang, J. Qiao, X. Hao, C. Zhang, J. Zhang, Y. Li, F. Huang and Y. Sun, *Adv. Energy Mater.*, 2022, **13,** 2103684.
25. J. Jia, Q. Huang, T. Jia, K. Zhang, J. Zhang, J. Miao, F. Huang and C. Yang, *Adv. Energy Mater.*, 2022, **12**, 2103193.
26. Y. Zhang, B. Wu, Y. He, W. Deng, J. Li, J. Li, N. Qiao, Y. Xing, X. Yuan, N. Li, C. J. Brabec, H. Wu, G. Lu, C. Duan, F. Huang and Y. Cao, *Nano Energy*, 2022, **93**, 106858.
27. T. Zhao, C. Cao, H. Wang, X. Shen, H. Lai, Y. Zhu, H. Chen, L. Han, T. Rehman and F. He, *Macromolecules*, 2021, **54**, 11468-11477.
28. C. Sun, J.-W. Lee, S. Seo, S. Lee, C. Wang, H. Li, Z. Tan, S.-K. Kwon, B. J. Kim and Y.-H. Kim, *Adv. Energy Mater.*, 2022, **12**, 2103239.
29. Z. Genene, J.-W. Lee, S.-W. Lee, Q. Chen, Z. Tan, B. A. Abdulahi, D. Yu, T.-S. Kim, B. J. Kim and E. Wang, *Adv. Mater.*, 2022, **34**, 2107361.
30. T. Jia, J. Zhang, H. Tang, J. Jia, K. Zhang, W. Deng, S. Dong and F. Huang, *Chem. Eng. J.*, 2022, **433**, 133575.
31. R. Ma, K. Zhou, Y. Sun, T. Liu, Y. Kan, Y. Xiao, T. A. Dela Peña, Y. Li, X. Zou, Z. Xing, Z. Luo, K. S. Wong, X. Lu, L. Ye, H. Yan and K. Gao, *Matter*, 2022, **5**, 725-734.

32. C. Cao, H. Wang, D. Qiu, T. Zhao, Y. Zhu, X. Lai, M. Pu, Y. Li, H. Li, H. Chen and F. He, *Adv. Funct. Mater.*, 2022, 2201828.
33. D. Chen, S. Liu, B. Huang, J. Oh, F. Wu, J. Liu, C. Yang, L. Chen and Y. Chen, *Small*, 2022, 2200734.
34. H. Yu, Y. Wang, H. K. Kim, X. Wu, Y. Li, Z. Yao, M. Pan, X. Zou, J. Zhang, S. Chen, D. Zhao, F. Huang, X. Lu, Z. Zhu and H. Yan, *Adv. Mater.*, 2022, 2200361.
35. H. Fu, Y. Li, Z. Wu, F. R. Lin, H. Y. Woo and A. K.-Y. Jen, *Macromol. Rapid Commun.*, 2022, 2200062.
36. T. Wang, R. Sun, X.-R. Yang, Y. Wu, W. Wang, Q. Li, C.-F. Zhang and J. Min, *Chinese J. Polym. Sci.*, 2022, DOI: 10.1007/s10118-022-2697-1.